ISSN 0036-0236, Russian Journal of Inorganic Chemistry, 2024. © Pleiades Publishing, Ltd., 2024.

INORGANIC MATERIALS AND NANOMATERIALS

Synthesis, Characterization, and Computational Studies of the Zinc Bromide Complex with 2-Amino-1,3,4-thiadiazole

K. Sh. Husenov[a], B. B. Umarov[b], K. K. Turgunov[c, d], B. Sh. Ganiev[b, *], U. M. Mardonov[a, b], B. T. Ibragimov[e], J. M. Ashurov[e], and D. A. Safin[f, g, **]

[a] *Navoi State University of Mining and Technologies, Navoi, 210100 Uzbekistan*

[b] *Bukhara State University, Bukhara, 200117 Uzbekistan*

[c] *Institute of Chemistry of Plant Substances named after S. Yu. Yunusov, Academy of Sciences of the Republic of Uzbekistan, Tashkent, 100170 Uzbekistan*

[d] *Turin Polytechnic University in Tashkent, Tashkent, 100125 Uzbekistan*

[e] *Institute of Bioorganic Chemistry, Uzbekistan Academy of Sciences, Tashkent, 700125 Uzbekistan*

[f] *University of Tyumen, Tyumen, 625003 Russia*

[g] *Scientific and Educational and Innovation Center for Chemical and Pharmaceutical Technologies, Ural Federal University named after the First President of Russia B.N. Yeltsin, Yekaterinburg, 620002 Russia*

**e-mail: b.sh.ganiyev@buxdu.uz*

***e-mail: damir.a.safin@gmail.com*

Received March 25, 2024; revised May 8, 2024; accepted May 8, 2024

Abstract—A new mononuclear heteroleptic complex bis(2-amino-1,3,4-thiadiazole-*N*)-dibromo zinc(II), $[ZnBr_2L_2]$ (**1**), which was obtained from 2-amino-1,3,4-thiadiazole (**L**), is reported. Complex **1** was studied by elemental analysis, FT-IR spectroscopy and single crystal X-ray diffraction. Crystal packing of complex **1** was additionally studied using the Hirshfeld surface analysis. The DFT/B3LYP/6-31++G(d,p) based computations were additionally applied to reveal electronic features of the obtained complex **1**. It was established that complex **1** contains two parent ligands **L**, which are monocoordinated through the thiadiazole 3-nitrogen atom and the coordination sphere of the metal cation is filled by two bromide anions. The molecular structure of complex **1** is stabilized by one N–H···N and one N–H···Br hydrogen bonds. Molecules of **1** are interlinked through a myriad of N–H···N and N–H···Br hydrogen bonds, and S···Br and π···π interactions, yielding a 3D supramolecular structure. Theoretical calculations revealed a strong electrophilic nature of the optimized structure of **1** with the most electro-rich and electron-deficient sites observed on the bromide anions and NH_2 hydrogen atoms, which are not involved in the formation of intramolecular hydrogen bonds, respectively.

Keywords: thiadiazole, zinc(II), heterocycle, X-ray, crystal structure, DFT

DOI: 10.1134/S0036023624600941

INTRODUCTION

It is impossible to imagine the nature without heterocyclic compounds, which pivotal role is hard to overestimate. Sufficing to mention that heterocycle-containing species constitute such vital molecules as DNA (deoxyribonucleic acid) and RNA (ribonucleic acid). Of a great myriad of heterocyclic compounds, five- and six-membered heterocycles, seem, to be the most widely spread. Furthermore, heterocyclic compounds, which are defined as cyclic compounds that have atoms of at least two different elements as members of its ring(s) [1, 2], are mainly constructed, besides the carbon atom, from nitrogen, oxygen and sulfur atoms. Of five-membered heterocyclic compounds, a promising class is the so-called azoles [3]. Thiadiazoles are, likely, one of most important building fragments for the fabrications of bioactive molecules [4, 5].

In continuation of our ongoing interest in heterocyclic compounds [6–13] as well as molecules with predicted potential biological activity [14–32], in this work we describe a new complex bis(2-amino-1,3,4-thiadiazole-*N*)-dibromo zinc(II), $[ZnBr_2L_2]$ (**1**), which was readily fabricated from a single-step addition reaction of 2-amino-1,3,4-thiadiazole (**L**) to $ZnBr_2 \cdot 2H_2O$ in the EtOH medium. Structural features of complex **1** were revealed using the FT-IR spectroscopy, single crystal X-ray diffraction and Hirshfeld surface analysis, while electronic properties were examined using the DFT computations. It should also be noted, that our comprehensive search in the Cambridge Structural Database (CSD) revealed only 12 hits for crystal structure of metallocomplexes with ligand **L**, namely $[ZnCl_2L_2]$ [33], $[ZnI_2L_2]$ [34], $[Zn(NO_3)_2L_3]$ [35], $[Zn(Lig)L(H_2O)_2] \cdot 2H_2O$ (Lig =

7-oxabicyclo[2.2.1]heptane-2,3-dicarboxylate)) [36], $(HL)_4[Sb_4Br_{16}]$ [37], $\{(HL)[BiI_4]\cdot L\}_n$ [38], $[Cu_4L_6](ClO_4)_4\cdot MeOH$ [39], $[Cu(Lig)L(H_2O)]$ (Lig = 2-[2-(1-anilino-1,3-dioxobutan-2-ylidene)hydrazin-1-id-1-yl]benzene-1-sulfonate) [40], [Cu(Lig)L] (Lig = 2-{2-[1-cyano-2-(imino)-2-methoxyethylidene]hydrazinyl}benzene-1-sulfonate) [41], $[Ag_4L_6](ClO_4)_4$ [39], $Co(Lig)L(H_2O)_2]\cdot 2H_2O$ (Lig = 7-oxabicyclo[2.2.1]heptane-2,3-dicarboxylate)) [36] and $[CdCl_2L]_n$ [42]. Thus, the coordination chemistry of **L** has poorly been studied.

EXPERIMENTAL

Materials and physical measurements. All reagents and solvents were commercially available and used as without further purification. The Fourier Transform Infrared (FT-IR) spectra were obtained using a Bruker Invenio ATR-S-2021 spectrometer in the range 400–4000 cm^{-1}. Elemental analysis was performed using a Carlo Erba EA 1108 elemental analyzer.

Synthesis of $[ZnBr_2L_2]$ (1). A hot solution of $ZnBr_2\cdot 2H_2O$ (0.784 g, 3 mmol) in EtOH (35 mL) was added to a hot solution of **L** (0.607 g, 6 mmol) in the same solvent (50 mL). The resulting mixture was refluxed under vigorous stirring for 1 h, followed by filtration and left undisturbed. Crystals suitable for single crystal X-ray diffraction were formed after about 2 days. Yield, 1.077 g (84%). FTIR (cm^{-1}): 1608, 1647, 3290, 3340, 3387 (NH_2). Anal. calcd. for $C_4H_6Br_2N_6S_2Zn$ (%): H, 1.41; C, 11.24; N, 19.66. Found (%): H, 1.40; C, 11.04; N, 19.29.

Hirshfeld surface analysis. The Hirshfeld molecular surface analysis [43–45] was performed to the corresponding crystal structure using the CrystalExplorer 21 software [46].

DFT calculations. Theoretical calculations were performed in gas phase using the Gaussian 09, Revision D.01 software package [47] and the GaussView 6.0 visualization software [48] using the density functional theory (DFT) method with Becke-3-parametr-Lee-Yang-Parr (B3LYP) hybrid functional [49, 50] and 6-311++G(d,p) basis set [49, 51]. The corresponding crystal structure geometry of the studied metal complex was used as a starting model for the optimization process. The vibration frequencies were calculated for the optimized structure in gas phase and no imaginary frequencies were obtained. HOMO and LUMO electronic isosurfaces, and molecular electrostatic potential surfaces were computed from the fully optimized structure.

X-ray diffraction. The X-ray diffraction data were collected at 293(2) K on a CCD Xcalibur Ruby (Oxford Diffraction) diffractometer (CuK_α, λ = 1.54184 Å, graphite monochromator). The structure was solved by direct methods using the program SHELXL-2014/7 [52] and refined by the full-matrix least-squares technique using SHELXL-2014/7 [52]. All non-hydrogen atoms were refined by the least squares method in the full-matrix anisotropic approximation. All CH hydrogen atom positions located on a difference map and included as fixed contributions riding on attached atoms with isotropic thermal parameters 1.2 times those of their carrier atoms. $C_4H_6Br_2N_6S_2Zn$, FW = 427.46 g mol^{-1}, monoclinic, space group $P2_1/n$, a = 7.9997(6) Å, b = 13.4283(8) Å, c = 11.4598(8) Å, β = 94.711(6)°, V = 1226.88(15) $Å^3$, Z = 4, ρ = 2.314 g cm^{-3}, $\mu(CuK_\alpha)$ = 13.443 mm^{-1}, reflections: collected 4842, unique 2478, R_{int} = 0.048, R_1(all) = 0.0779, wR_2(all) = 0.1233, S = 1.014.

CCDC 2089098 contains the crystallographic data. These data can be obtained free of charge via https://www.ccdc.cam.ac.uk/structures or from the Cambridge Crystallographic Data Centre, 12 Union Road, Cambridge CB2 1EZ, UK; fax: (+44)-1223-336-033; or e-mail: deposit@ccdc.cam.ac.uk.

RESULTS AND DISCUSSION

The reaction of two equivalents of **L** with one equivalent of $ZnBr_2\cdot 2H_2O$ in ethanol allowed to produce a new mononuclear heteroleptic complex $[ZnBr_2L_2]$ (**1**) (Scheme 1), which composition is fully supported by the elemental analysis data.

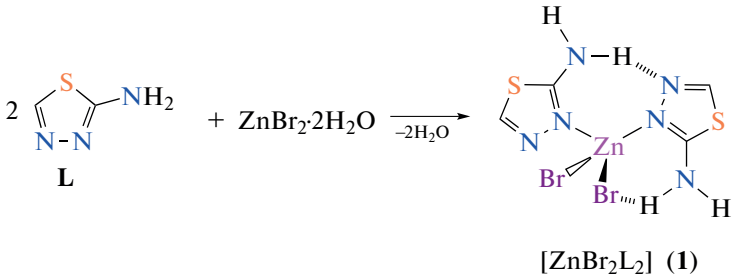

$[ZnBr_2L_2]$ (**1**)

Scheme 1. Synthesis of **1**.

The FTIR spectrum of complex **1** is, in general, resembles the corresponding spectrum of the parent ligand **L**; however, some changes can clearly be observed due to coordination of **L** to $ZnBr_2$ (Fig. 1). In

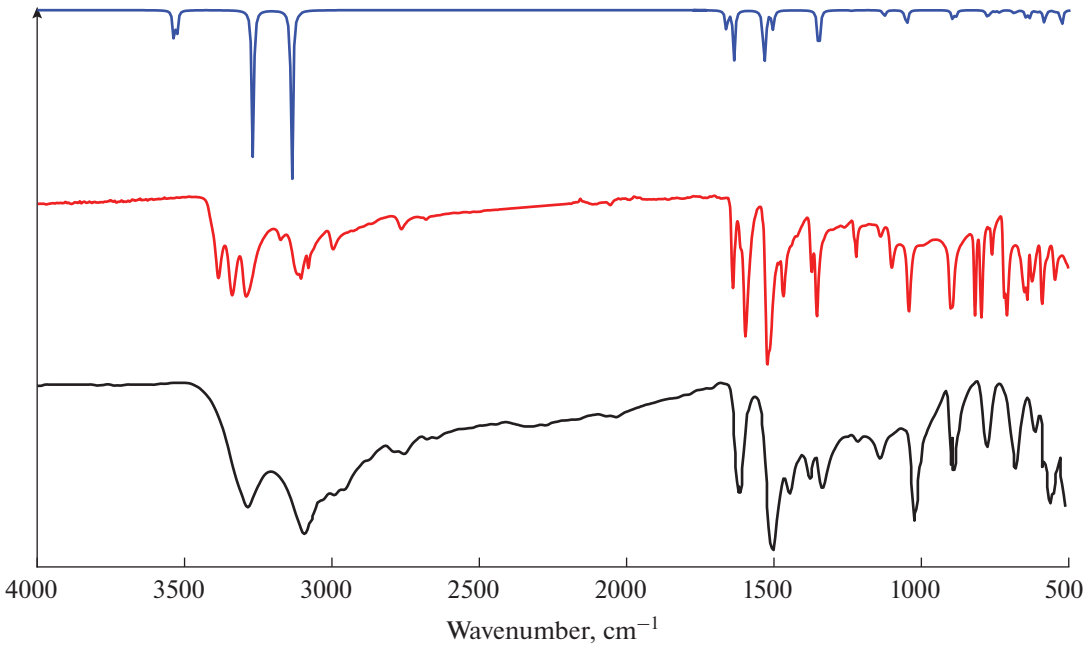

Fig. 1. Experimental FT-IR spectra of **L** (black) and **1** (red), and calculated spectrum of **1** (blue).

particular, the NH_2 groups in the spectrum of complex are shown as three resolved bands at 3200–3450 cm^{-1}, and two bands at 1608 and 1647 cm^{-1} due to stretching and bending vibrations, respectively, while in the spectrum of **L** the same group is shown as a single broad band at 3285 cm^{-1} and a band at 1620 cm^{-1}. The observed splitting of the NH_2 bands can be explained by the participation of these groups in the formation of different intra- and intermolecular hydrogen bonds as it is evidenced from the crystal structure of **1** (vide infra).

Complex **1** crystallized in monoclinic space group $P2_1/n$ with one complex molecule $[ZnBr_2L_2]$ in the asymmetric unit. Both ligands **L** in the molecular structure of **1** are monocoordinated through the thiadiazole 3-nitrogen atom and the coordination sphere of the metal cation is filled by two bromide anions, all together yielding a four-membered N_2Br_2 coordination environment (Fig. 2). The coordination polyhedron in the structure of **1** is characterized by the so-called τ_4-descriptor of 0.9404. Note, that the τ_4 values for perfect square planar, seesaw, trigonal pyramid and tetrahedral structures are 0.00, 0.07–0.64, 0.85 and 1.00, respectively. Thus, the coordination polyhedron is best described as being about 40% along the pathway of distortion from the ideal tetrahedral toward trigonal pyramidal structure.

The Zn–N bond lengths are about 2.01–2.04 Å, while the Zn–Br bonds are about 0.4 Å longer (Table 1). The N–N and C–S bonds within the thiadiazole rings are about 1.37–1.39 and 1.72–1.74 Å, respectively. Interestingly, the C–N bonds, formed with the corresponding coordinated nitrogen atoms, are about 1.32 Å and very similar to those formed with the NH_2 nitrogen atoms, which are about 1.32–1.34 Å. The same bonds, formed with the noncoordinated nitrogen atoms of the thiadiazole rings, are about 0.05 Å shorter. Notably, all the bond lengths within the ligands **L** in the structure of the discussed complex are very similar to those of the previously reported derivatives $[ZnHal_2L_2]$ (Hal = Cl [33], I [34]), while the Zn–Br bonds are about 0.14 Å longer and about 0.19 Å shorter in comparison to the Zn–Cl and Zn–I bonds, respectively. The N–Zn–N and Br–Zn–Br bond angles in the structure of **1** are very similar and of about 114°, while the N–Zn–Br bond angles slightly lower and of about 106°–110°. These bond angles are very similar to those in the structures of $[ZnHal_2L_2]$ (Hal = Cl [33], I [34]). Finally, the dihedral angle formed by the mean planes of the two thiadiazole rings is 7.2(3)°.

The molecular structure of complex **1** is stabilized by one N–H···N and one N–H···Br hydrogen bonds (Fig. 3, Table 2). Molecules of **1** are interlinked through a myriad of N–H···N and N–H···Br hydrogen bonds, and S···Br and π···π interactions, yielding a 3D supramolecular structure. The latter interactions are formed by both sides of one of the thiadiazole fragments, while the second thiadiazole fragment is involved into the formation of π···π interactions through one of its sides.

Crystal packing of complex **1** was additionally analyzed using the Hirshfeld surface analysis implemented within the CrystalExplorer 21 software. As evidenced from the corresponding 2D fingerprint

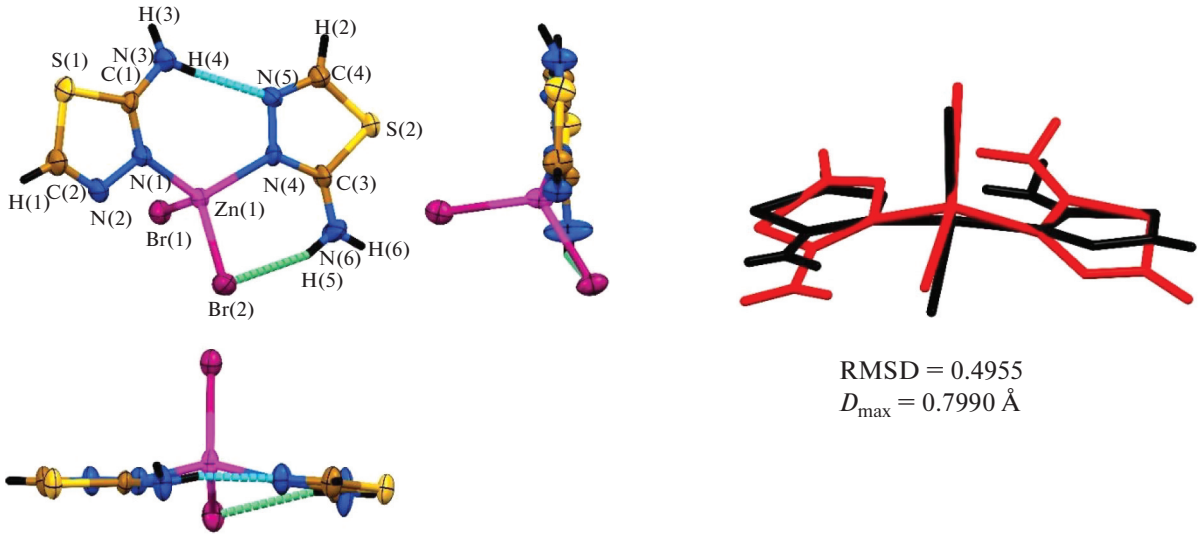

Fig. 2. (left) Different views on the molecular structure of **1**. Color code: N–H···N hydrogen bond = cyan dashed line, N–H···Br hydrogen bond = green dashed line. (right) Overlay of the molecular (black) and optimized (red) structures of **1**.

plots, reciprocal H···Br, H···H, S···Br and H···N contacts are the dominant contributors to the molecular surface, all together comprising 67.1% of this surface (Fig. 4, Table 3). Notably, the H···Br and H···N contacts are shown on the corresponding 2D fingerprint plots as a pair of symmetric horns with the shortest values at $d_e + d_i \approx 2.6$ and 2.4 Å, respectively, corresponding to the above described intermolecular N–H···Br and N–H···N hydrogen bonds (Fig. 3, Table 2). The reciprocal S···Br contact on the corresponding 2D fingerprint plot are shown as a pair of closely adjacent spikes with the shortest $d_e + d_i \approx 3.3$ Å (Fig. 4), corresponding to the above-mentioned intermolecular S···Br interactions. The second group of dominant contacts on the molecular surface of **1** includes reciprocal H···S, N···S, C···S, C···N, N···Br, H···C and C···C contacts, all together comprising 30.1% of the surface. The reciprocal N···S, C···S, C···N and C···C contacts are shown in the corresponding 2D fingerprint plots as the characteristic areas on the diagonal at $d_e = d_i \approx 1.8$–2.4 Å and correspond to the above discussed π···π interactions formed between the thiadi-

Table 1. Selected bond lengths (Å), bond angles and dihedral angles (deg) in the crystal and optimized structures of **1** (see Fig. 2 for atoms labelling)

	Experimental	Calculated		Experimental	Calculated
Bond length					
Zn–N(1)	2.014(5)	2.130	C(1)–N(3)	1.336(9)	1.344
Zn–N(4)	2.043(5)	2.174	C(1)–S(1)	1.726(7)	1.754
Zn–Br(1)	2.4000(12)	2.381	C(2)–S(1)	1.736(7)	1.759
Zn–Br(2)	2.3926(12)	2.394	C(3)–N(4)	1.322(8)	1.323
N(1)–N(2)	1.390(8)	1.372	C(4)–N(5)	1.286(9)	1.286
N(4)–N(5)	1.370(7)	1.369	C(3)–N(6)	1.318(10)	1.337
C(1)–N(1)	1.320(8)	1.323	C(3)–S(2)	1.740(6)	1.761
C(2)–N(2)	1.272(9)	1.283	C(4)–S(2)	1.716(7)	1.753
Bond angle					
N(1)–Zn–N(4)	114.0(2)	101.54	N(4)–Zn–Br(1)	105.72(14)	103.17
N(1)–Zn–Br(1)	106.59(16)	104.58	N(4)–Zn–Br(2)	106.95(14)	105.10
N(1)–Zn–Br(2)	110.25(15)	112.81	Br(1)–Zn–Br(2)	113.40(4)	126.54
Dihedral angle					
Thiadiazole···Thiadiazole				7.2(3)	33.31

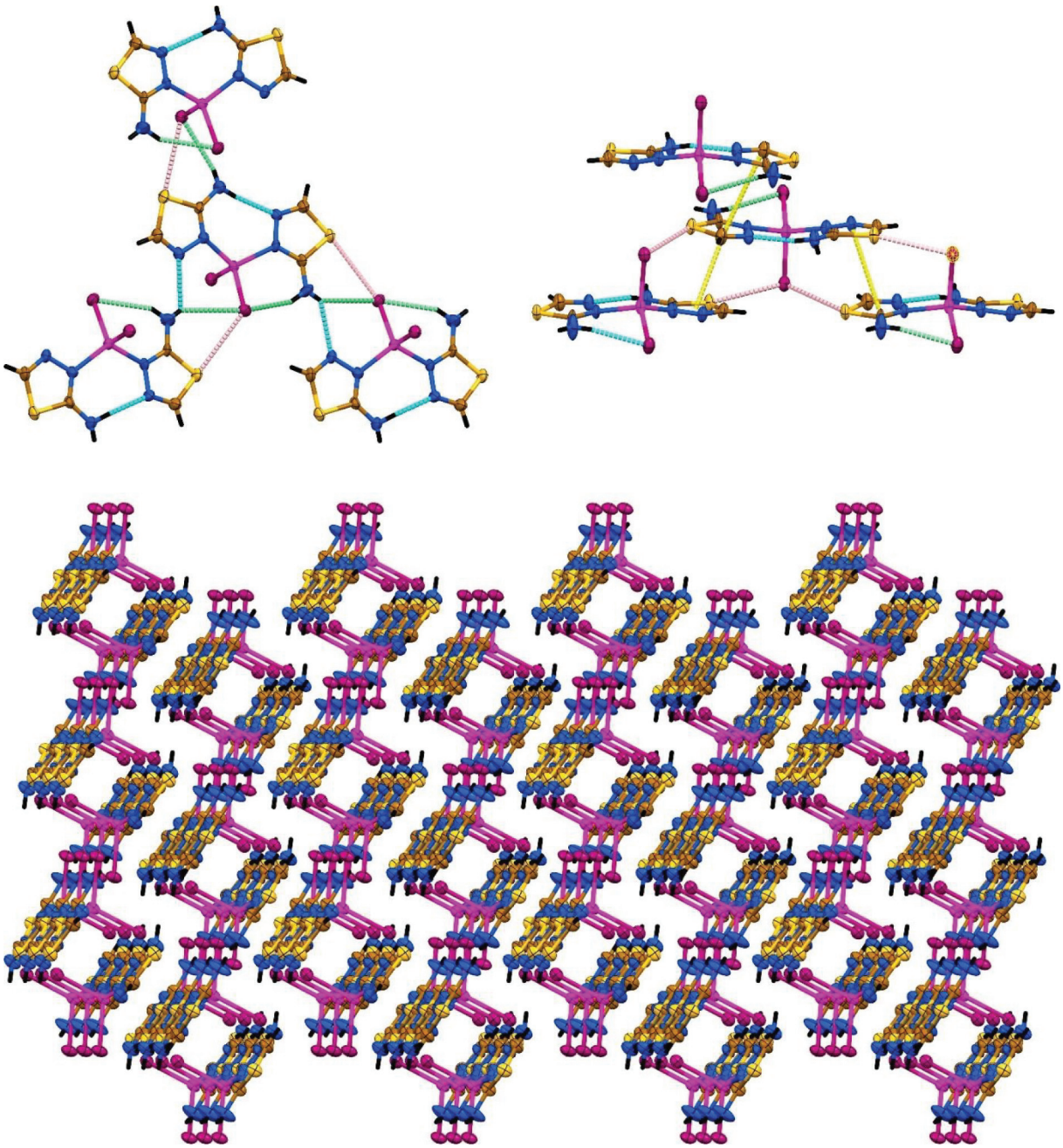

Fig. 3. (top) Views on the supramolecular clusters, constructed through intermolecular N–H···N, N–H···Br hydrogen bonds and S···Br interactions (left), and through S···Br and π···π interactions (right), in the crystal structure of **1**. (bottom) Crystal packing in the structure of **1**. Color code: H = black, C = gold, N = blue, S = yellow, Br = purple, Zn = magenta; N–H···N hydrogen bond = cyan dashed line, N–H···Br hydrogen bond = green dashed line, S···Br interaction = pink dashed line, π···π interaction = yellow dashed line.

azole rings (Fig. 3, Table 2). Remaining reciprocal contacts, namely N···N, C···Br, Br···Br, S···S, Zn···S, Zn···C and Zn···S, all together comprising about 2.8% of the molecular surface, are very minor contributors, each occupying <0.8% of the total surface (Table 3). The reciprocal H···N, H···Br, C···N, C···S, N···S and S···Br contacts in the crystal structure of **1** are highly favoured since the corresponding enrichment ratios E_{HN}, E_{HBr}, E_{CN}, E_{CS}, E_{NS} and E_{SBr} are larger than unity. This is explained by a relatively higher proportion of these contacts on the total Hirshfeld surface area over a corresponding proportion of random contacts. The reciprocal H···H, H···S, N···Br, H···C, N···N, C···Br, S···S and Br···Br contacts are much less favoured or even impoverished since the corresponding enrichment ratios are signifi-

Table 2. Hydrogen bond, Br···S and π···π interaction lengths (Å) and angles (deg) in the crystal structure of **1**[a]

	Hydrogen bond						
	D–H···A	*d*(D–H)	*d*(H···A)	*d*(D···A)			∠(DHA)
Experimental	N(3)–H(4)···N(3)	0.89(5)	2.08(5)	2.956(9)			168(5)
	N(3)–H(3)···Br(1)$^{\#1}$	0.88(9)	2.74(10)	3.442(7)			138(9)
	N(6)–H(6)···N(2)$^{\#2}$	0.76(7)	2.54(6)	3.080(9)			129(6)
	N(6)–H(5)···Br(2)	0.90(9)	2.57(9)	3.404(8)			154(7)
	N(6)–H(6)···Br(2)$^{\#2}$	0.76(7)	2.89(7)	3.531(8)			144(6)
Calculated	N(3)–H(4)···N(3)	1.021	2.070	3.028			155.41
	N(6)–H(5)···Br(2)	1.028	2.336	3.325			160.98
	Br···S interaction						
	Br(1)···S(1)$^{\#3}$			3.4865(18)			
	Br(1)···S(1)$^{\#1}$			3.6684(18)			
	Br(1)···S(2)$^{\#4}$			3.3999(17)			
	Br(2)···S(2)$^{\#5}$			3.5985(18)			
	π···π interaction						
	Cg(*I*)	Cg(*J*)	*d*(Cg(*I*)···Cg(*J*))	α	β	γ	Slippage
	Thiadiazole$_{S1}$	Thiadiazole$_{S2}$$^{\#4}$	3.659(3)	5.7(3)	18.2	17.0	1.145
	Thiadiazole$_{S2}$	Thiadiazole$_{S1}$$^{\#3}$	3.659(3)	5.7(3)	17.0	18.2	1.070
	Thiadiazole$_{S2}$	Thiadiazole$_{S2}$$^{\#6}$	3.588(3)	0.0(3)	18.3	18.3	1.127

[a] Symmetry operation: $^{\#1}$ $-1/2 + x$, $1/2 - y$, $1/2 + z$; $^{\#2}$ $3/2 + x$, $1/2 + y$, $1/2 - z$; $^{\#3}$ $1/2 - x$, $1/2 + y$, $1/2 - z$; $^{\#4}$ $1/2 - x$, $-1/2 + y$, $1/2 - z$; $^{\#5}$ $3/2 - x$, $-1/2 + y$, $1/2 - z$; $^{\#6}$ $1 - x$, $1 - y$, $1 - z$.

Table 3. Hirshfeld contact surfaces and derived "random contacts" and "enrichment ratios" for **1**

	H	C	N	S	Br	Zn
	Contacts (*C*, %)[a]					
H	13.4	–	–	–	–	–
C	2.5	1.0	–	–	–	–
N	13.0	4.0	0.7	–	–	–
S	7.8	4.9	6.3	0.3	–	–
Br	27.5	0.6	3.6	13.2	0.4	–
Zn	0.3	0.2	0.0	0.2	0.0	0.0
	Surface (*S*, %)					
	39.0	7.1	14.2	16.5	22.9	0.4
	Random contacts (*R*, %)					
H	15.2	–	–	–	–	–
C	5.5	0.5	–	–	–	–
N	11.0	2.0	2.0	–	–	–
S	12.9	2.3	4.7	2.7	–	–
Br	17.8	3.2	6.5	7.5	5.2	–
Zn	0.3	0.0	0.1	0.1	0.2	0.0
	Enrichment (*E*)[b]					
H	0.88	–	–	–	–	–
C	0.45	–	–	–	–	–
N	1.18	1.99	0.35	–	–	–
S	0.61	2.09	1.35	0.11	–	–
Br	1.54	0.18	0.56	1.75	0.08	–
Zn	–	–	–	–	–	–

[a] Values are obtained from CrystalExplorer 21 [46].
[b] The "enrichment ratios" were not computed when the "random contacts" were lower than 0.9% as they are not meaningful [45].

cantly less than unity and of 0.08–0.88. Thus, the obtained results of the Hirshfeld surface analysis of intermolecular contacts in the crystal structure of **1** strongly support the dominant role of the intermolecular N–H···N and N–H···Br hydrogen bonds as well as S···Br interactions and π···π interactions between the thiadiazole rings in the crystal packing.

We have further revealed energy frameworks to additionally analyze the overall crystal packing of complex **1**. For this purpose, a molecular cluster of radius 3.8 Å was considered within the CrystalExplorer 21 software. As evidenced from the obtained results, the electrostatic energy component is the dominant one for the molecules linked through the N–H···Br and S···Br interactions, molecules linked through the π···π interactions with the longer distances (3.659(3) Å) between the thiadiazole centroids, and molecules linked through the N–H···N, N–H···Br and S···Br interactions (Fig. 5, Table 4). Notably, the latter two types of molecules with the mentioned interactions are linked with the most favourable values of the total energies. A similar total energy value was revealed for the molecules interacting through the π···π interactions with the shorter distance (3.588(3) Å) between the thiadiazole centroids; however, the dispersion energy component in this case is the dominant one followed by the electrostatic one. The next intermolecular interactions dominated by the dispersion

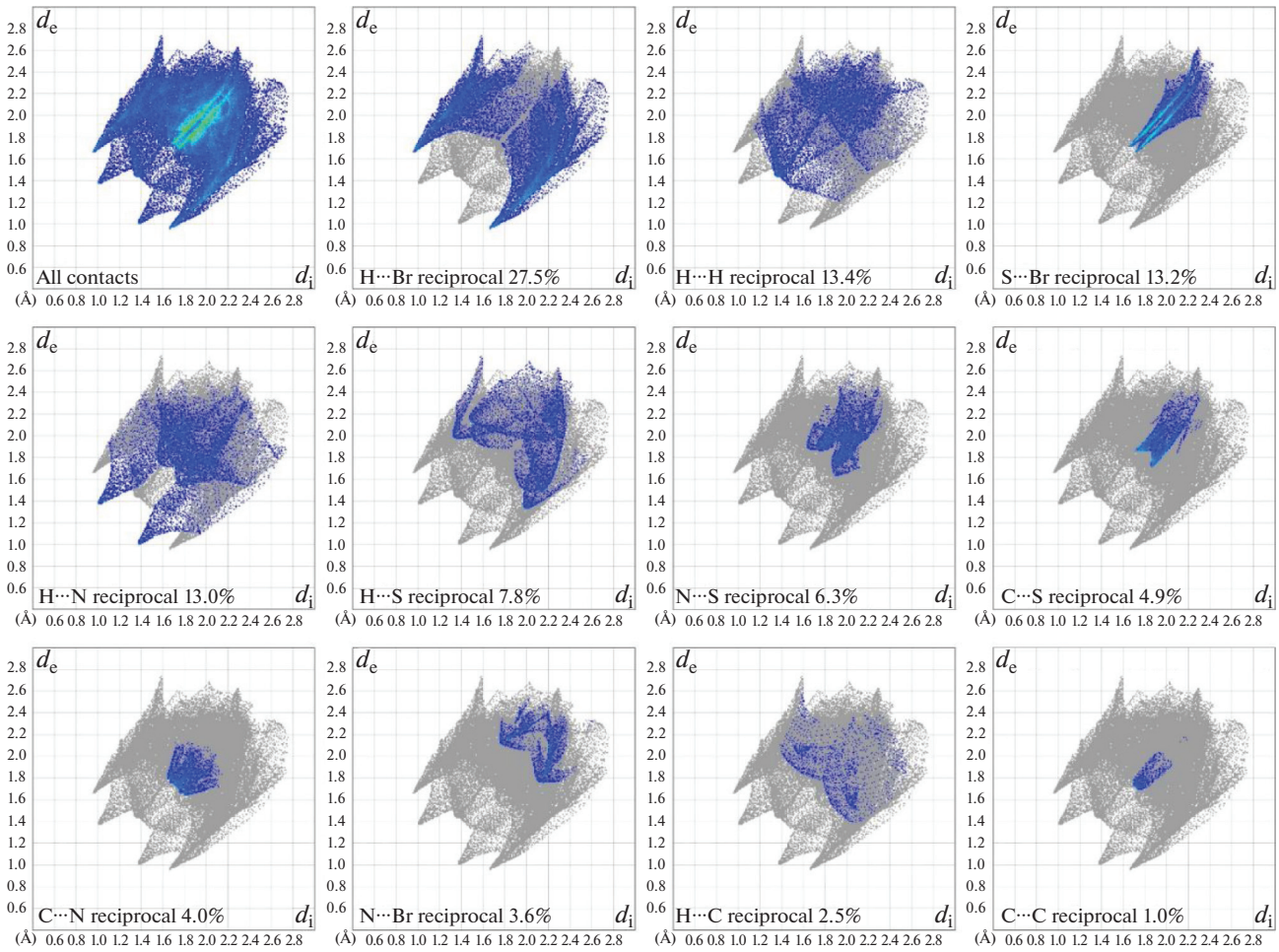

Fig. 4. 2D fingerprint plots of the main contacts in the structure of **1**.

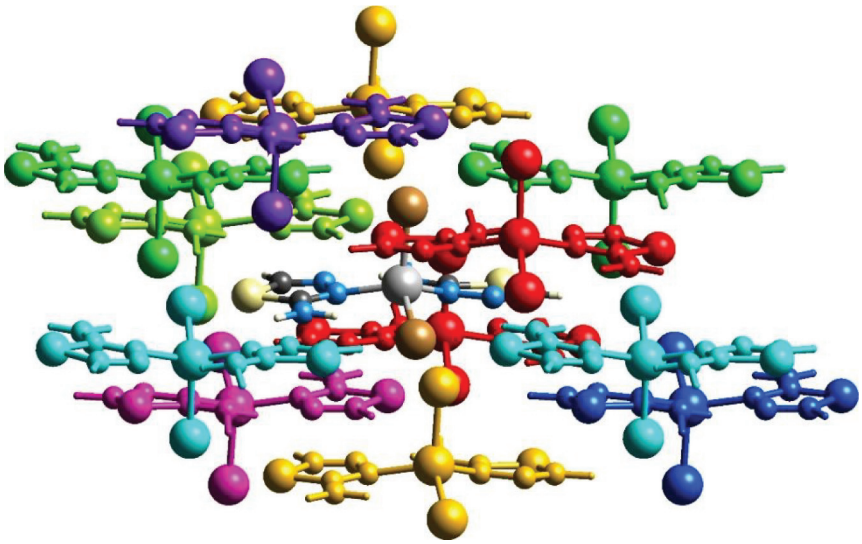

Fig. 5. The color-coded interaction mapping within 3.8 Å of the centering molecule in the crystal structure of **1**, calculated from a single-point molecular wavefunction at B3LYP/6-31G(d,p).

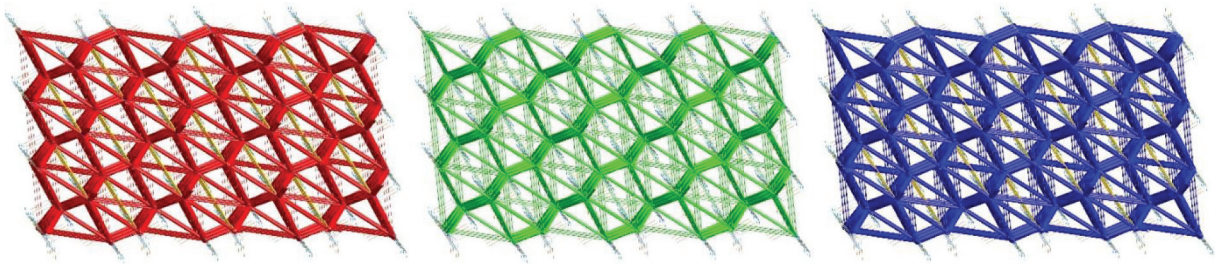

Fig. 6. Frameworks for electrostatic (left), dispersion (middle) and total (right) energies computed for the crystal structure of **1**. The cylindrical diameters reflect the relative contribution of the corresponding energies, and they were adjusted to the same scale factor of 50 within 3 × 3 × 4 unit cells.

energy component were revealed for the molecules linked through the weak N–H···Br interactions (3.09(10) Å) and weak π···π interactions with the distance between the thiadiazole centroids of 4.957(3) Å and slippage of 3.827 Å. The other dispersion energy component dominated interactions were found for the molecules interacting through the weak N–H···H–C dihydrogen interactions, although the total energy is highly positive and mainly dictated by the positive electrostatic component. The corresponding energy frameworks are shown in Fig. 6.

The structure of complex **1** was further optimized using the DFT-based computations to examine its electronic features. The calculated bond lengths and bond angles are in good agreement with the experimental ones (Fig. 2, Table 1); however, clear discrepancies of about 13° are observed between the experimental and calculated values for the N(1)–Zn–N(4) and Br(1)–Zn–Br(2) bond angles (Table 1). This is also reflected in the values of the dihedral angle between the two thiadiazole rings (Fig. 2, Table 1). The calculated dipole moment of a molecule of **1** is high and of ~9.38 Debye with the largest contribution from the μ_y component of about –7.82 Debye followed by the μ_z component of about –4.99 Debye (Table 5).

Analysis of the Mulliken charges of atoms of complex **1** revealed that all the hydrogen atoms are positively charged with the highest (~0.40) and lowest (~0.20) charges observed on the NH_2 hydrogen atoms H(4) and H(5) (Fig. 7), which are involved in the formation of the intramolecular N(3)–H(4)···N(5) and N(6)–H(5)···Br(2) hydrogen bonds, respectively (Fig. 2, Table 2). In general, the most positive and negative charges of about 0.81 and –0.48 were found on the Zn(II) cation and the bromide anion Br(1) (Fig. 7). The second most negative charge of about –0.44 was found on the second bromide anion Br(2), which is involved in the formation of the intramolecular N(6)–H(5)···Br(2) hydrogen bond (Fig. 2, Table 2). Both coordinated nitrogen atoms N(1) and N(4) carry a low positive charge of about 0.06 and 0.12 (Fig. 7). The other positively charged atom is the sulfur atom (~0.05) of the thiadiazole ligand, which forms two intramolecular hydrogen bonds (Fig. 2, Table 2). Remaining nonhydrogen atoms of both ligands **L** are negatively charged from about –0.04 to –0.35 (Fig. 7).

Table 4. Interaction energies (kJ/mol) calculated with the B3LYP/6-31G(d,p) energy model for the crystal structure of **1**. Values in parenthesis are obtained after normalizing to 100% the sum of the attractive energy contributions

	N^a	Symmetry operation	R	E^b_{ele}	E^b_{pol}	E^b_{dis}	E^b_{rep}	E^b_{tot}
	2	$x + 1/2, -y + 1/2, z + 1/2$	7.70	–36.7 (54.3)	–10.5 (15.5)	–20.4 (30.2)	41.1	–38.9
	2	x, y, z	8.00	–3.9 (19.6)	–5.8 (29.1)	–10.2 (51.3)	7.4	–12.7
	1	$-x, -y, -z$	10.33	19.8	–2.6 (36.1)	–4.6 (63.9)	0.4	15.2
	2	$-x + 1/2, y + 1/2, -z + 1/2$	7.68	–66.3 (54.3)	–17.7 (14.5)	–38.2 (31.3)	75.3	–69.9
	2	$-x + 1/2, y + 1/2, -z + 1/2$	8.05	–64.0 (63.6)	–14.3 (14.2)	–22.3 (22.2)	42.2	–71.6
	1	$-x, -y, -z$	10.53	–7.3 (39.0)	–1.6 (8.6)	–9.8 (52.4)	7.2	–13.0
	1	$-x, -y, -z$	7.75	–20.4 (59.6)	–5.7 (16.7)	–8.1 (23.7)	2.1	–31.5
	1	$-x, -y, -z$	6.40	–39.7 (38.8)	–8.4 (8.2)	–54.1 (52.9)	44.6	–67.8

[a] N is the number of molecules with an R molecular centroid-to-centroid distance (Å); color codes in the first column are referenced to Fig. 5.
[b] E_{ele} is the electrostatic energy, E_{pol} is the polarization energy, E_{dis} is the dispersion energy, E_{rep} is the exchange-repulsion energy, k values are scale factors; $E_{tot} = k_{ele} \times E_{ele} + k_{pol} \times E_{pol} + k_{dis} \times E_{dis} + k_{rep} \times E_{rep} = 1.057 \times E_{ele} + 0.740 \times E_{pol} + 0.871 \times E_{dis} + 0.618 \times E_{rep}$ [53].

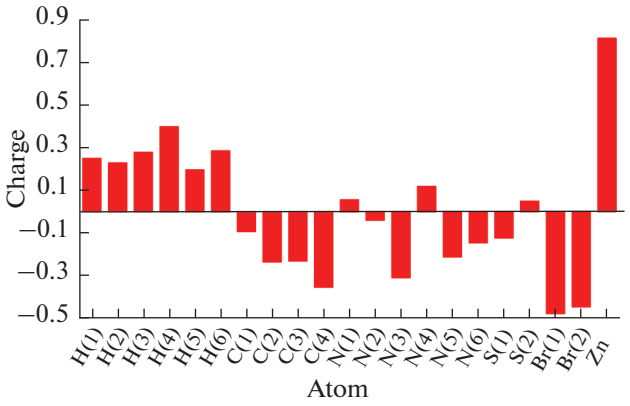

Fig. 7. Mulliken atomic charges in the optimized structure of complex **1** (see Fig. 2 for atoms labelling).

The HOMO in the molecule of complex **1** was found to be delocalized on the $ZnBr_2$ fragment, the nitrogen atom of the NH_2 group, which is involved in the formation of the N–H···N hydrogen bond, and the coordinated nitrogen atom of the same ligand **L** (Fig. 8). The LUMO is delocalized on the second ligand **L** and the C(NH_2) carbon atom of the other ligand **L** (Fig. 8).

The HOMO and LUMO values also dictate the ionization energy (I) and electron affinity (A). The obtained values of I and A indicate relatively low electron donating and electron accepting properties of the optimized molecule of **1** (Table 5). Furthermore, **1** is characterized by a relatively high value of η and a relatively low value of S, indicating this complex exhibits a tendency not to exchange its electron cloud with surrounding environment. The electrophilicity index (ω) value is about 3.61 eV, which is in the range for the pronounced electrophiles. Finally, the optimized structure of **1** can accept about 1.76 electrons as evidenced from the corresponding ΔN_{max} values.

Table 5. Dipole moments, frontier molecular orbitals, gap values and descriptors for the optimized structure of complex **1**

μ_D, Debye	9.3774
μ_x, Debye	1.4056
μ_y, Debye	–7.8164
μ_z, Debye	–4.9864
E_{HOMO}, eV	–6.408
E_{LUMO}, eV	–1.771
$\Delta E_{LUMO-HOMO} = E_{LUMO} - E_{HOMO}$, eV	4.637
Ionization energy, $I = -E_{HOMO}$, eV	6.408
Electron affinity, $A = -E_{LUMO}$, eV	1.771
Electronegativity, $\chi = (I + A)/2$, eV	4.090
Chemical potential, $\mu = -\chi$, eV	–4.090
Global chemical hardness, $\eta = (I - A)/2$, eV	2.319
Global chemical softness, $S = 1/(2\eta)$, eV^{-1}	0.216
Global electrophilicity index, $\omega = \mu^2/(2\eta)$, eV	3.607
$\Delta N_{max} = -\mu/\eta$	1.764

We have also calculated the molecular electrostatic potential (MEP) surface of the optimized structure of complex **1**, which revealed two bromide anions, followed by the noncoordinated thiadiazole nitrogen atom of the ligand **L**, which is not involved in the formation of the intramolecular N–H···Br hydrogen bond, as the most electron-rich sites (Fig. 9). The most electron deficient sites were found on the hydrogen atoms of both NH_2 fragments, which are not involved into N–H···N and N–H···Br hydrogen bonds.

The molecule of complex **1** comprises 21 atoms, thus exhibiting 57 normal modes in the IR spectrum. The calculated IR spectrum is in good agreement with the experimental one (Fig. 1). Bands for the stretching vibrations of the NH fragments, not involved in the formation of intramolecular N–H···N and N–H···Br hydrogen bonds, were shown at 3524 and 3538 cm^{-1}, while the stretching bands of the NH fragments involved in the formation of intramolecular N–H···N and N–H···Br hydrogen bonds were shown at 3269 and 3134 cm^{-1}, respectively. Band for the NH bending vibrations were found at 1635 and 1663 cm^{-1}. The CN fragments of the ligands **L** were revealed in the spectrum as two bands at 1504 and 1531 cm^{-1}, while the CS vibrations were shown as a band at 1352 cm^{-1}.

CONCLUSIONS

In conclusion, a new mononuclear heteroleptic coordination compound bis(2-amino-1,3,4-thiadiazole-*N*)-dibromo zinc(II), [$ZnBr_2L_2$] (**1**), which was readily obtained from the addition reaction of two equivalents of 2-amino-1,3,4-thiadiazole (**L**) to one equivalent of $ZnBr_2 \cdot 2H_2O$, is reported. The composition of the obtained complex was proved by the means of elemental analysis, and its structure was revealed by FT-IR spectroscopy and single crystal X-ray diffraction. Crystal packing of complex **1** was additionally studied using the Hirshfeld surface analysis. In a molecule of **1**, two parent ligands **L** are monocoordinated through the thiadiazole 3-nitrogen atom and the coordination sphere of the metal cation is filled by two bromide anions, all together yielding a four-membered N_2Br_2 coordination environment, which is best described as being about 40% along the pathway of distortion from the ideal tetrahedral toward trigonal pyramidal structure. The molecular structure of complex **1** is stabilized by one N–H···N and one N–H···Br hydrogen bonds. Molecules of **1** are interlinked through a myriad of N–H···N and N–H···Br hydrogen bonds, and S···Br and π···π interactions, yielding a 3D supramolecular structure. The molecular surface

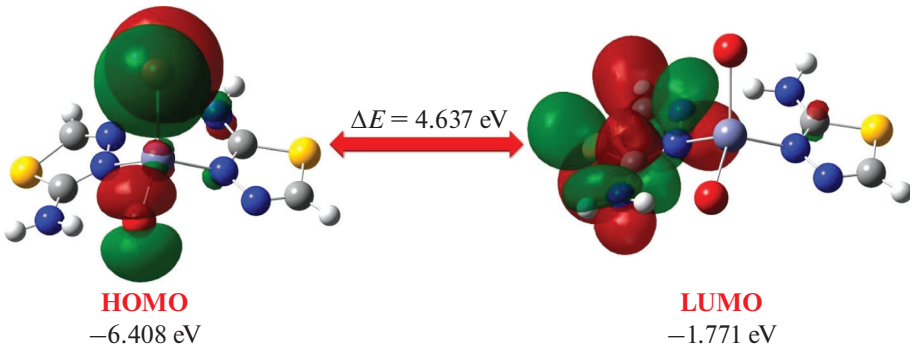

Fig. 8. The HOMO and LUMO of the optimized structure of complex **1**.

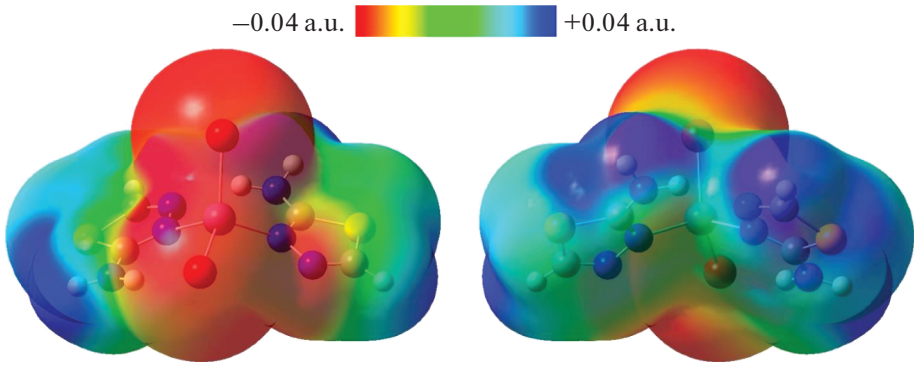

Fig. 9. Front and rare views on the molecular electrostatic potential (MEP) surface of the optimized structure of complex **1**.

of **1** is described by highly favoured reciprocal H···N, H···Br, C···N, C···S, N···S and S···Br contacts. The DFT/B3LYP/6-31++G(d,p) based calculations revealed a strong electrophilic nature of the optimized structure of **1** with the bromide anions being the most nucleophilic sites and NH_2 hydrogen atoms, which are not involved in the formation of intramolecular hydrogen bonds, being the most electrophilic sites. Finally, the crystal structure of complex **1** reported herein fills the previously incomplete series of the related complexes $[ZnHal_2L_2]$ (Hal = Cl [33], I [34]). Thus, the reported herein complex **1** together with its chlorine and iodine derivatives are of potential interest to further detailed studies of their properties of value, e.g. optical and catalytic.

FUNDING

This work was supported by ongoing institutional funding. no additional grants to carry out or direct this particular research were obtained.

CONFLICT OF INTEREST

The authors of this work declare that they have no conflicts of interest.

REFERENCES

1. https://goldbook.iupac.org/terms/view/H02798.
2. G. P. Moss, P. A. S. Smith, and D. Tavernier, Pure Appl. Chem. **67**, 1307 (1995).
3. J. A. Maertens, Clin. Microbiol. Infect. **10**, 1 (2004).
4. Y. Hu, C.-Y. Li, X.-M. Wang, Y.-H. Yang, and H.-L. Zhu, Chem. Rev. **114**, 5572 (2014).
5. A. K. Jain, S. Sharma, A. Vaidya, V. Ravichandran, and R. K. Agrawal, Chem. Biol. Drug. Des. **81**, 557 (2013).
6. D. A. Safin, Y. Xu, I. Korobkov, D. L. Bryce, and M. Murugesu, CrystEngComm **15**, 10419 (2013).
7. D. A. Safin, K. Burgess, I. Korobkov, D. L. Bryce, and M. Murugesu, CrystEngComm **16**, 3466 (2014).
8. D. A. Safin, N. A. Tumanov, A. A. Leitch, J. L. Brusso, Y. Filinchuk, and M. Murugesu, CrystEngComm **17**, 2190 (2015).
9. D. A. Safin, R. J. Holmberg, K. M. N. Burgess, K. Robeyns, D. L. Bryce, and M. Murugesu, Eur. J. Inorg. Chem. 441 (2015).
10. D. A. Safin, A. Pialat, I. Korobkov, and M. Murugesu, Chem. Eur. J. **16**, 6144 (2015).
11. D. A. Safin, A. Pialat, A. Leitch, N. A. Tumanov, I. Korobkov, Y. Filinchuk, J. L. Brusso, and M. Murugesu, Chem. Commun. **51**, 9547 (2015).
12. D. A. Safin, P. M. J. Szell, A. Keller, I. Korobkov, D. L. Bryce, and M. Murugesu, New J. Chem. **39**, 7147 (2015).

13. D. A. Safin, J. M. Frost, and M. Murugesu, Dalton Trans. **44**, 20287 (2015).
14. B. Ay, O. Şahin, B. Saygıdeğer Demir, Y. Saygideger, J. M. López-de-Luzuriaga, G. Mahmoudi, and D. A. Safin, New J. Chem. **44**, 9064 (2020).
15. L. E. Alkhimova, M. G. Babashkina, and D. A. Safin, Tetrahedron **97**, 132376 (2021).
16. M. G. Babashkina, A. Frontera, A. V. Kertman, Y. Saygideger, S. Murugavel, and D. A. Safin, J. Iran. Chem. Soc. **19**, 85 (2022).
17. L. E. Alkhimova, M. G. Babashkina, and D. A. Safin, J. Mol. Struct. **1251**, 131975 (2022).
18. L. E. Alkhimova, T. M. Burkhanova, M. G. Babashkina, and D. A. Safin, Tetrahedron **109**, 132671 (2022).
19. A. V. Sharov, T. M. Burkhanova, T. Taskin Tok, M. G. Babashkina, and D. A. Safin, Int. J. Mol. Sci. **23**, 1508 (2022).
20. A. I. Krysantieva, J. K. Voronina, and D. A. Safin, Int. J. Mol. Sci. **24**, 4660 (2023).
21. R. A. Omar, P. Koparir, K. Sarac, M. Koparir, and D. A. Safin, J. Chem. Sci. **135**, 6 (2023).
22. N. A. Garkusha, O. P. Anikeeva, I. Bayıl, T. Taskin-Tok, and D. A. Safin, J. Indian Chem. Soc. **100**, 100926 (2023).
23. L. E. Alkhimova, A. V. Sharov, T. M. Burkhanova, M. G. Babashkina, and D. A. Safin, Polycycl. Aromat. Comp. **43**, 2599 (2023).
24. M. G. Babashkina, and D. A. Safin, Polycycl. Aromat. Comp. **43**, 3324 (2023).
25. M. G. Babashkina, T. Taskin-Tok, T. M. Burkhanova, and D. A. Safin, Polycycl. Aromat. Comp. **43**, 4729 (2023).
26. P. Koparir, R. A. Omar, K. Sarac, L. O. Ahmed, A. Karatepe, T. Taskin-Tok, and D. A. Safin, Polycycl. Aromat. Compd. **43**, 6107 (2023).
27. T. M. Burkhanova, A. I. Krysantieva, M. G. Babashkina, I. A. Konyaeva, L. N. Monina, A. N. Goncharenko, and D. A. Safin, Struct. Chem. **34**, 1545 (2023).
28. I. Garcia-Santos, A. Castiñeiras, B. Eftekhari Sis, G. Mahmoudi, and D. A. Safin, Polyhedron **235**, 116362 (2023).
29. R. A. Omar, P. Koparir, M. Koparir, and D. A. Safin, J. Sulfur Chem. **45**, 120 (2024).
30. T. Taskin-Tok, and D. A. Safin, Monatsh. Chem. **155**, 57 (2024).
31. D. A. Safin, C. R. Chim., accepted for publication.
32. D. A. Safin, Russ. J. Phys. Chem. A **98**, 221 (2024).
33. K. Sh. Khusenov, B. B. Umarov, M. M. Ishankhodzhaeva, N. A. Parpiev, S. A. Talipov, and B. T. Ibragimov, Russ. J. Coord. Chem. **23**, 555 (1997).
34. M. M. Ishankhodzhaeva, K. Sh. Khusenov, B. B. Umarov, et al., Russ. J. Inorg. Chem. **43**, 1709 (1998).
35. K. Sh. Khusenov, B. B. Umarov, M. M. Ishankhodzhaeva, N. A. Parpiev, S. A. Talipov, and B. T. Ibragimov, Russ. J. Inorg. Chem. **43**, 1841 (1998).
36. N. Wang, Q.-Y. Lin, J. Feng, Y.-L. Zhao, Y.-J. Wang, and S.-K. Li, Inorg. Chim. Acta **363**, 3399 (2010).
37. L. Antolini, A. Benedetti, A. C. Fabretti, and A. Giusti, J. Chem. Soc., Dalton Trans. **2501**, 2501 (1988).
38. A. Cornia, A. C. Fabretti, R. Grandi, and W. Malavasi, J. Chem. Cryst. **24**, 277 (1994).
39. M. Maekawa, M. Munakata, T. Kuroda-Sowa, Y. Suenaga, and K. Sugimoto, Inorg. Chim. Acta **290**, 153 (1999).
40. A. V. Gurbanov, G. Mahmoudi, M. Fatima C. Guedes da Silva, F. I. Zubkov, K. T. Mahmudov, and A. J. L. Pombeiro, Inorg. Chim. Acta **471**, 130 (2018).
41. A. V. Gurbanov, V. A. Aliyeva, R. M. Gomila, A. Frontera, K. T. Mahmudov, and A. J. L. Pombeiro, Cryst. Gowth Des. **23**, 7335 (2023).
42. M.-C. Suen, C.-W. Yeh, and C.-H. Jou, Acta Cryst. **E67**, m1082 (2011).
43. M. A. Spackman, and J. J. McKinnon, CrystEngComm **4**, 378 (2002).
44. M. A. Spackman, and D. Jayatilaka, CrystEngComm **11**, 19 (2009).
45. C. Jelsch, K. Ejsmont, and L. Huder, IUCrJ **1**, 119 (2014).
46. P. R. Spackman, M. J. Turner, J. J. McKinnon, S. K. Wolff, D. J. Grimwood, D. Jayatilaka, and M. A. Spackman, J. Appl. Crystallogr. **54**, 1006 (2021).
47. M. J. Frisch, G. W. Trucks, H. B. Schlegel, G. E. Scuseria, M. A. Robb, J. R. Cheeseman, G. Scalmani, V. Barone, B. Mennucci, G. A. Petersson, H. Nakatsuji, M. Caricato, X. Li, H. P. Hratchian, A. F. Izmaylov, J. Bloino, G. Zheng, J. L. Sonnenberg, M. Hada, M. Ehara, K. Toyota, R. Fukuda, J. Hasegawa, M. Ishida, T. Nakajima, Y. Honda, O. Kitao, H. Nakai, T. Vreven, J. A. Montgomery Jr., J. E. Peralta, F. Ogliaro, M. Bearpark, J. J. Heyd, E. Brothers, K. N. Kudin, V. N. Staroverov, T. Keith, R. Kobayashi, J. Normand, K. Raghavachari, A. Rendell, J. C. Burant, S. S. Iyengar, J. Tomasi, M. Cossi, N. Rega, J. M. Millam, M. Klene, J. E. Knox, J. B. Cross, V. Bakken, C. Adamo, J. Jaramillo, R. Gomperts, R. E. Stratmann, O. Yazyev, A. J. Austin, R. Cammi, C. Pomelli, J. W. Ochterski, R. L. Martin, K. Morokuma, V. G. Zakrzewski, G. A. Voth, P. Salvador, J. J. Dannenberg, S. Dapprich, A. D. Daniels, O. Farkas, J. B. Foresman, J. V. Ortiz, J. Cioslowski, and D. J. Fox, Gaussian 09, Revision D.01, 2013.
48. R. Dennington, T. A. Keith, and J. M. Millam, GaussView, Version 6.0; Semichem Inc., Shawnee Mission: Shawnee, Kansas (2016).
49. R. Krishnan, J. S. Binkley, R. Seeger, and J. A. Pople, J. Chem. Phys. **72**, 650 (1980).
50. A. D. Becke, J. Chem. Phys. **98**, 5648 (1993).
51. M. J. Frisch, J. A. Pople, and J. S. Binkley, J. Chem. Phys. **80**, 3265 (1984).
52. G. M. Sheldrick, Acta Cryst. **A71**, 3 (2015).
53. C. F. Mackenzie, P. R. Spackman, D. Jayatilaka, and M. A. Spackman, IUCrJ **4**, 575 (2017).

Publisher's Note. Pleiades Publishing remains neutral with regard to jurisdictional claims in published maps and institutional affiliations.